Anomalous Perturbation of the O_2 Sensitivity of Poly(aromatic) Hydrocarbons by Magnetic Quantum Dots

Asra Hassan, Armen Shamirian, Xi Zhang, and Preston T. Snee[*]

Department of Chemistry, University of Illinois at Chicago, 845 West Taylor Street, Chicago, Illinois 60607-7061, United States

KEYWORDS quantum dots, dopant, pyrene, fluorescence, delayed fluorescence, molecular oxygen, sensing.

ABSTRACT

Molecular oxygen is known to be an efficient quencher of the excited states of organic molecules. This fact has been exploited to develop fluorescent O_2 sensors, which is topical for cancer screening and many other applications. In this regard, our group and others have reported the development of robust, ratiometrically reporting chemosensors by conjugating O_2-sensitive organic chromophores to inorganic quantum dots. Recently, an attempt was made to prepare a multifunctional sensor system by attaching the emissive poly(aromatic) hydrocarbons pyrene and perylene to magnetic nanomaterials, specifically CdSe/CdMnZnS and ZnSe/ZnMnS/ZnS quantum dots. However, the fluorescence of both dyes became invariant to oxygen levels, even if the

solutions were fully saturated. We have ruled out any material dependency beyond the presence of Mn^{2+} ions by studying control samples, while molecular dynamics simulations negated any possibility of spatial sequestration of O_2 by the magnetic fields. In the case of pyrene, the proximity of the magnetic dots induces significant singlet-triplet mixing; however, this does not explain this curious observation. As such, we believe that the exchange interaction between O_2 and the dyes is perturbed by both the microenvironment of the system and the inhomogeneous magnetic fields such that quenching is not observed.

1. INTRODUCTION

The quantification of oxygen levels is important in variety of fields such as clinical and environmental analysis.[1] Therefore, many examples of fluorescent O_2 sensors have been reported that function via the quenching of the lowest electronically excited singlet and triplet states of various luminophores by ground state molecular oxygen.[2] Several groups have incorporated fluorescent quantum dots (QDs, or nanocrystals) for oxygen sensing applications due to their unique optical properties, such as narrow and tunable emission, high quantum yield, and resistance to photobleaching.[3,4] However, high quality QDs are almost universally prepared with an inorganic shell to passivate their surfaces.[5,6] As a result, QDs are intrinsically insensitive to their environment. A solution is to conjugate the QDs to small analyte-sensitive chromophores to create dual-emissive systems that ratiometrically report analyte concentration. In the case of O_2 sensing, there are many examples of oxygen-sensitive dye-QD coupled chromophores.[7-12] Fluorescent functionalized poly(aromatic) hydrocarbons (PAHs), such as pyrene and perylene, are highly suitable for use in this regard as long as they can be derivatized for conjugation to colloidal nanocrystals.

Our group has recently reported a QD-based ratiometric fluorescent O_2 sensor that was successfully applied for analysis in live cells.[9] During these investigations, several combinations of O_2-sensitive chromophores coupled to a variety water-soluble quantum dots were prepared and examined. To our surprise, the use of a magnetic nanomaterial rendered the organic components' emissions to be invariant with respect to the oxygen levels. This report describes the discovery of this effect and probes the nature of the dye-dot interactions that are potentially responsible, as well as how such O_2-insensitivity may be harnessed for analytical applications.

2. EXPERIMENTAL

2.1 Materials and methods. All chemicals are used as received unless noted. Triphenylphosphine (99%) was purchased from Alfa Aesar. Poly(ethylene glycol (MW: 600) was purchased from Fluka. Technical grade 1-octadecene (90%), bis-trimethylsilyl sulfide (purum, >98%), 1-pyrenebutyric acid N-hydroxysuccinimide ester (95%), manganese chloride (>99%), sodium hydroxide (97%), and triethylamine (>99.5%) were purchased from Sigma-Aldrich. Zinc acetate (99%) and n-decylamine (99%) were purchased from Acros. Stearic acid (≥97%) was purchased from Fluka. Diethylzinc (95%) was purchased from Strem. 1-Ethyl-3-(3-dimethylaminopropyl)carbodiimide (EDC) was purchased from Advanced ChemTech. L-lysine was purchased from Chem-Impex. Benzotriazole-1-yl-oxy-tris-(dimethylamino)-phosphonium hexafluorophosphate (BOP) was purchased from Nova Biochem. Heterobifunctional N_3-PEG-NH_2 was prepared by the protocol of ref. 13. Common solvents were purchased from Fisher. Poly(ethylene glycol) carbodiimide was prepared according to ref. 14. Manganese stearate was prepared according to ref. 15.

2.2. AminoPEG-functionalized 1-pyrenebutyric acid and perylene synthesis. Scheme 1 outlines the following procedure to prepare a conjugatable, water-soluble pyrene derivative.

Approximately 7 mL of DMF was used to dissolve 0.25 g 1-pyrenebutyric acid N-hydroxysuccinimide ester (0.65 mmol) with 0.404 g N_3-PEG-NH_2 (0.65 mmol). The solution was stirred under a N_2 atmosphere. The next day, the solvent was removed under vacuum. The resulting solid was purified by flash chromatography over silica using a mobile phase of dichloromethane. The purified precursor was dissolved in 10 mL of THF into which 0.163 g triphenylphosphine (0.62 mmol) was added. After 4 hr stirring at room temperature, ~0.5 g water was added and the solution was stirred for another 12 hr. The next day, the solvent was removed under vacuum, and ~5 mL water was added. To purify the final product, the solution was acidified using HCl in a separatory funnel. Three portions of 50 mL methylene chloride were added to extract the byproducts. The product in the collected organic portion was extracted with ~100 mL 0.1 M HCl solution. After neutralization with diluted NaOH, the product was extracted back into methylene chloride and dried. Flash chromatography was used to purify the product using methylene chloride (95% v/v) with 5% dry, distilled methanol over alumina. The purified product is a brown-yellow viscous solid (yield: 56%) and emits a very bright blue light under a UV lamp. NMR and optical characterizations are provided in Figures S1 and S2, respectively, in the supporting information. The perylene dye derivative was prepared exactly as reported in ref. 9.

2.3. CdSe/CdZnS, ZnSe/ZnMnS/ZnS, and ZnSe/ZnS/ZnS QD synthesis. All procedures to produce CdSe/CdZnS dots can be found in the supporting information of ref. 16. The synthesis of ZnSe/ZnMnS/ZnS is described in ref. 17. ZnSe/ZnS/ZnS QDs were prepared by the same protocol; however, no manganese precursors were added in the 1st shell growth, the absence of which was accounted for by additional zinc precursors.

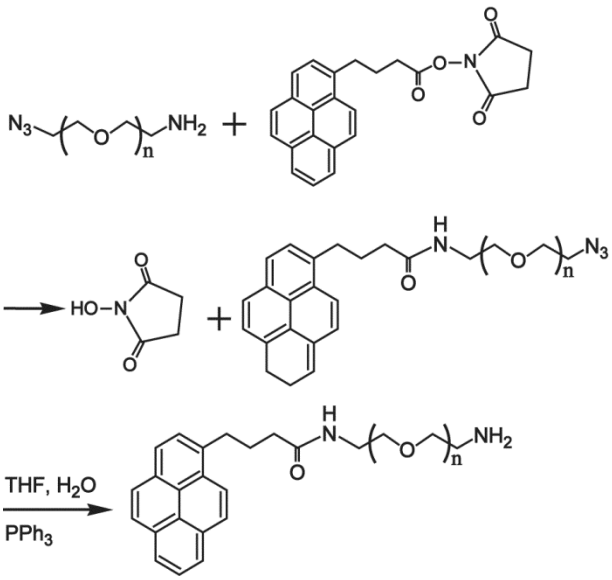

Scheme 1. Scheme for the preparation of aminoPEG-functionalized 1-pyrenebutyric acid.

2.4. Synthesis of CdSe core / magnetically doped shell QDs. Core CdSe QDs were synthesized based on a previously published procedure.[16] CdSe/CdMnS QDs were prepared according to the report of Chen et al. with the addition of manganese stearate during the shell growth process. The synthesis of CdSe/CdMnZnS is reported here. To overcoat the core with a magnetic shell, a solution of 3.383 g distilled trioctylphosphine oxide, 3.4 mL trioctylphosphine, 25 mg cadmium acetate dihydrate (0.108 mmol) and 0.5 g tetradecylphosphonic acid (1.8 mmol) were added to a 4-neck 100 mL round bottom flask. The solution was degassed at ~100 °C, heated to 250 °C under N_2, cooled back ~100 °C, and degassed again. A portion of the core dots were purified with precipitation and dissolved in hexane, which was added with a small (10% relative to Zn) level of manganese stearate to the overcoating solution at ~80 °C and degassed. Next 2.8 mL decylamine was added under a strong flow of N_2 and the solution was allowed to stir for ~ 2 hours at 80 °C. Next, the temperature was raised to 220 °C after which two solutions of 15 mg diethyl zinc (0.122 mmol) and 35 mg bis-trimethylsilyl sulfide (0.196 mmol), each dissolved in 3 mL TOP, were

separately injected over the course of 2 hours. All precursor quantities were calculated to achieve a 5 monolayer coverage for the quantity of core QDs being coated.

2.5 Quantum dot functionalization. The aminoPEG-functionalized 1-pyrenebutyric acid dye was conjugated to QDs with poly(ethylene glycol) carbodiimide using protocol discussed in ref. 14. Typical concentrations of CdSe/CdZnS QDs were 0.1 μM with 2-3 decades excess aminoPEG-functionalized pyrene and activator. Unconjugated pyrene dye was removed with Millipore concentrating filters (100 kDa MWCO) using basic (0.1 M NaOH) water; typical conjugation yields were 10% → 20%.

2.6 Characterization. UV/Vis absorbance spectra were taken using a Varian Cary 300 Bio UV/Vis spectrophotometer. Fluorescence emission spectra were taken using a customized Fluorolog (HORIBA Jobin Yvon) modular spectrofluorometer. An EPR spectrum was measured with a Varian E-109E spectrometer. Time resolved emission and dynamics were measured using a home-built system consisting of a NL-100 Nitrogen laser excitation source to produce emission that was fed into a Jarrell Ash monochromator, the output of which was measured by an Applied Photophysics PMT coupled to a Tektronix tds5104b digital phosphor oscilloscope (1GHz). The PMT was powered by a FLUKE 412B high voltage power supply.

When measuring emission, the absorbance of all solutions was kept near or below 0.1 OD at the excited wavelength to avoid inner-filtering effects. Excitation was set between 335 nm to 360 nm to co-excite the pyrene and QDs simultaneously and 420 nm for perylene-QD conjugates.

2.7 Molecular Dynamics Simulations. To determine the effect of a magnetic field on the dynamics of O_2, a molecular dynamics simulation was performed using 2000 SPC/E water molecules[18] surrounding a $Zn_{138}S_{138}$ nanoparticle. The coordinates of the cluster were taken from the optimized geometry of a $Cd_{138}S_{138}(H_2CO_2)_{24}$ quantum dot using DFT with the PBE1/PBE

hybrid functional[19,20] and the SBJKC basis set and effective core potentials.[21] This model was chosen due to the fact that a CdZnS shell on a CdSe particle grows quasi-epitaxially,[22] and thus the crystal parameters for CdS are an appropriate representation. The Lennard-Jones (LJ) parameters for ZnS were taken from ref. 23, charges from ref. 24, while the O_2 LJ parameters were from ref. 25. Full Ewald sums were used for the long-range electrostatic interactions. The calculations were performed using in-house software, which was verified to perform correctly by testing the properties of SPC/E water to demonstrate that correct dynamical averages were obtained (diffusion constant, enthalpy of vaporization, etc.). The system was equilibrated for ~100 ps, after which a trajectory of 140 ps was performed to characterize the average force on the O_2 molecule. Next, the trajectory was reinitiated from the beginning with an additional magnetic force on one of the O_2 atoms towards the nearest Zn center. The net force was simulated to be the maximum aligned magnetic dipoles. There were no discernible differences in the dynamics after 40 ps. The magnitude of the force was arbitrarily multiplied by 10× to represent the presence of more Mn centers, yet the O_2 trajectory with and without this force was essentially identical.

3. RESULTS / DISCUSSION

This study began by sensibly constructing dual-emitting chromophore systems where one component is responsive to oxygen while another functions as a reference, here a quantum dot. Several O_2-sensitive chromophores exist that are efficiently quenched by molecular oxygen. Among these, poly(aromatic) hydrocarbons are often employed as they have interesting and complex luminescent features. For example, pyrene emits with sharp fluorescence bands in the UV/blue-visible (~320 nm - 450 nm) in addition to a broad and structureless feature in the blue-green region (~400 nm - 550 nm) that appears at higher concentrations, see Figure 1B. The latter can also be observed by conjugating multiple copies of the dye to a singular nanostructure to create

a high local concentration, see Figure 2. This low energy feature is due to excimer emission from an excited singlet state pyrene - ground state pyrene dimer. Further complicating matters is the phenomenon of delayed fluorescence, which is the result of triplet-triplet annihilation.[26] This process occurs due to energy transfer between two interacting excited triplet state molecules to produce a dimer in the excited singlet excimer state. This results in the observation of excimer emission over a long, triplet-lifetime timescale which is the delayed fluorescence process. These dynamics are outlined in Figure 1A, which represents the interconnections between the excited singlet S* (blue), excimer S_2* (green), and triplet T (red) states that create the rich emission spectra shown in Figure 1B.

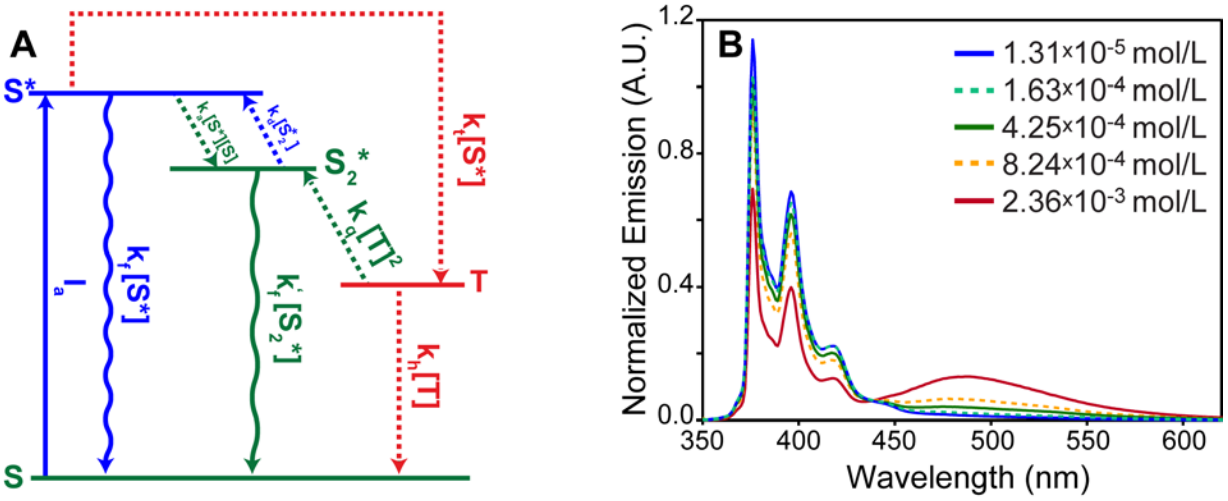

Figure 1. A. Jablonski diagram illustrating normal and delayed fluorescence of pyrene, adapted from ref. 26. The following symbologies are used: I_a: Excitation rate. k_f and k'_f: Radiative singlet monomer and dimer relaxation rates, respectively; the non-radiative pathways are not represented for clarity. k_q: Bimolecular triplet-triplet quenching rate. k_t: Intersystem crossing rate. k_h: Nonradiative triplet relaxation rate. k_a: Bimolecular singlet association rate. k_d: Excided singlet dimer dissociation rate. **B.** Normalized emission from aminoPEG-functionalized pyrene in water demonstrates concentration-dependent excimer emission.

One system that was explored initially is in essence a water-soluble version of the oxygen-sensitive probe reported by Amelia et al.[8] A poly(ethylene glycol)-pyrene chromophore was prepared by conjugating 1-pyrenebutyric acid to a heterobifunctional PEG linker. The first studies were conducted by coupling this dye to polymer-encapsulated CdSe/CdZnS QDs as the photophysical behavior of these nanomaterials is well established. Upwards of ~100 pyrene chromophores were conjugated per QD using high-yielding protocols.[14,27] As shown in Figure 2A, the emission of a chromophore with a low pyrene:QD ratio (~20) displays a QD feature at the semiconductor bandgap at ~595 nm and sharp pyrene breathing modes from 350 nm to 450 nm. When the pyrene: QD ratio was increased to ~100:1, the broad excimer emission centered at ~480 nm forms due to the dimerization of the dye on the QD surface.[28] This is evident from the fact that excimer emission is observed regardless of how much the coupled chromophores are diluted as shown in Figure 2B.

The sensitivity of the coupled pyrene-QD conjugates towards oxygen was measured. The sample was sparged with N_2 for ~1 hr, after which time the cuvette was covered and the emission was promptly measured. The same protocol was followed after saturating the solution with oxygen. The spectra in Figure 3 demonstrate oxygen sensitivity via the quenching of pyrene in the presence of oxygen. Combined with the QD insensitivity towards O_2, the result is a self-calibrating signal that can be used to make measurements in a biological milieu as we recently demonstrated in live HeLa cells using perylene-$AgInS_2$/ZnS QD coupled chromophores.[9] As with this previous study, we next sought to use a Cd-free quantum dot component to enhance biological compatibility. To this end the aminoPEG-functionalized pyrene derivative was conjugated to nontoxic ZnSe/ZnMnS/ZnS QDs.[17] However, the results were inexplicable- *there was no response observed to the saturation of O_2* as shown in Figure 4A.

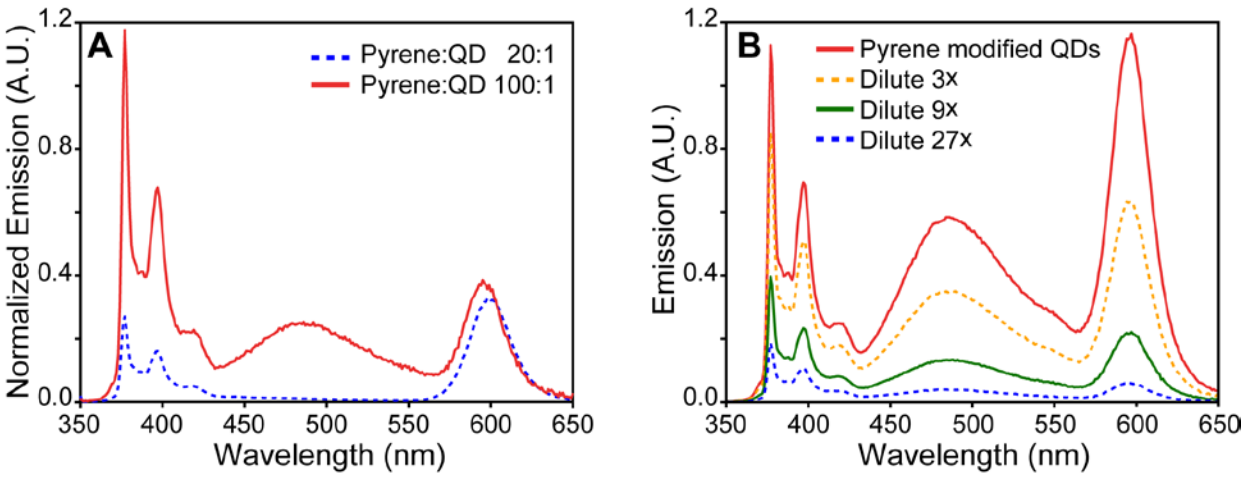

Figure 2: **A.** A 20:1 pyrene to QD coupled chromophore does not have a high enough dye loading ratio to result in excimer emission, which is observed in the 100:1 conjugate. Spectra have been normalized to the QD signal at 595 nm after subtracting pyrene's excimer component. **B.** The emission spectra of pyrene-QD coupled chromophore as a function of dilution demonstrate that excimer emission is present far below (~1000×) the critical micelle concentration of aminoPEG-functionalized pyrene (~1.6×10^{-4} M, see Figure 1B).

To examine this issue of the non-sensitivity, we studied each component of the pyrene-ZnSe/ZnMnS/ZnS QD construct individually. First, note that the dots are doped with manganese transition metal ions that act as visible-emitting phosphors. Not only does this alter the QD's optical properties,[15,29,30] the ions are highly magnetic as well. As a result, our hypothesis is that the presence of Mn^{2+} in the shell inhibited pyrene from sensing oxygen via a magnetic interaction. This was explored by synthesizing undoped water-soluble pyrene-ZnSe/ZnS/ZnS QDs. It was found that pyrene is efficiently quenched by oxygen when conjugated to these non-magnetic dots, which eliminates the possibility of a material dependence beyond the influence of manganese ions (see Figure S3 of the supporting information). To further verify that Mn^{2+} is the culprit, core / doped shell Cd-based QDs were prepared given that no odd behavior was observed previously in

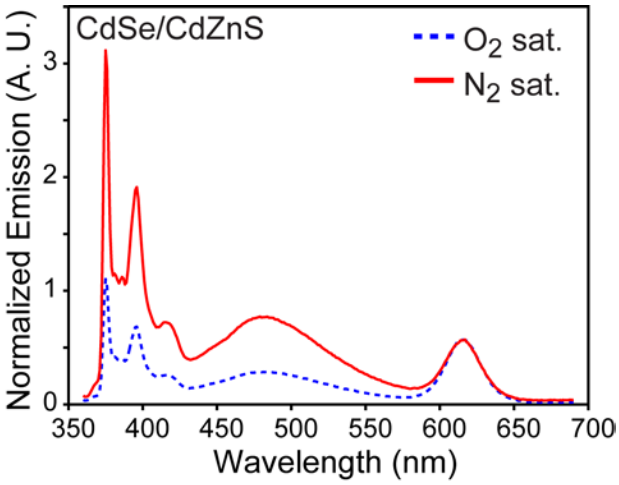

Figure 3: The emission spectra of pyrene-functionalized CdSe/CdZnS QDs after saturating with N_2 and O_2 demonstrate ratiometric fluorescent oxygen-sensing capability. Spectra have been normalized to the QD emission intensity.

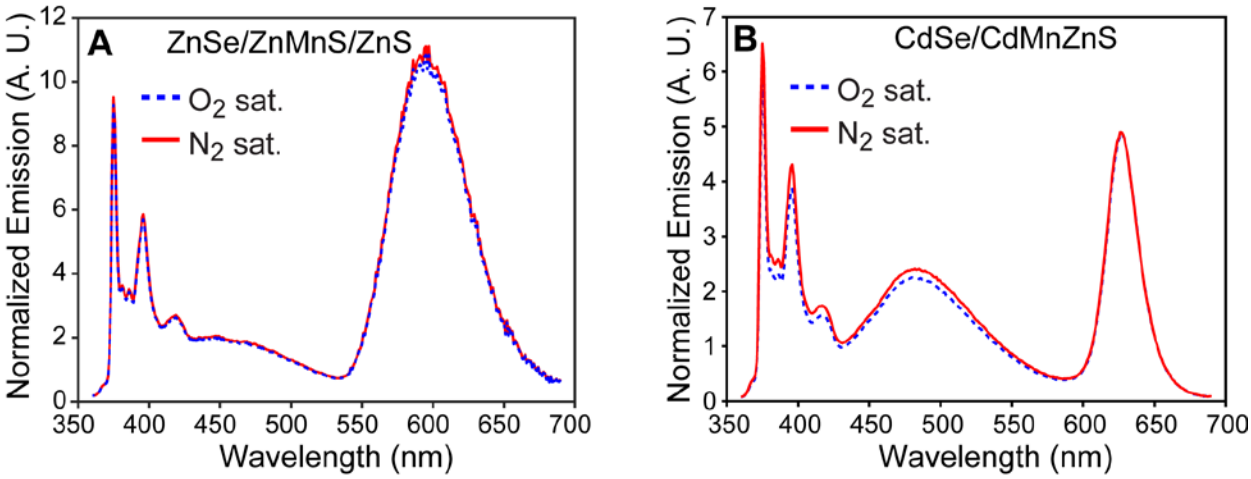

Figure 4: A. The emission spectra of pyrene-functionalized ZnSe/ZnMnS/ZnS QDs after saturating with O_2 and N_2. **B.** The emission spectra of pyrene-functionalized CdSe/CdMnZnS QDs after saturating with N_2 and O_2. All spectra have been normalized to the QD emission intensity after subtraction of the dye component.

pyrene-CdSe/CdZnS dots as shown in Figure 3. To this end several synthetic strategies were examined, beginning with an attempt to prepare CdSe/CdMnS dots via an alteration of the

procedure reported by Chen et. al.[31] This synthetic protocol is of fundamental interest due to the resulting narrow and symmetric emission spectra, which is unusually good for a core/shell material. Although we were able to reproduce these properties, it was found that doping this system results in fairly low photoluminescence quantum yields (QYs), see supporting information Table S1. Hence, another protocol was developed to shell-doped CdSe/CdMnZnS dots, which ultimately resulted in magnetic QDs with substantially higher QYs. Electron paramagnetic resonance (Figure S4) measurements confirm the presence of Mn^{2+}.

CdSe/CdMnZnS QDs were water-solubilized and functionalized with pyrene. In agreement with our previous results, the organic chromophore minimally responded at best to saturation of the solution with oxygen as shown in Figure 4B. Several investigations were conducted to further explore this odd phenomenon. Another functionalized PAH, aminoPEG-functionalized perylene that was employed in our previous study,[9] was coupled to magnetic CdSe/CdMnZnS QDs. Again, the chromophore was minimally quenched by saturating the solution with oxygen, see the supporting information for details. To verify that the sparging of the dots was not responsible, enzymatic removal of O_2 via the oxidation of glucose with glucose oxidase was employed.[9] The same results were obtained- the PAHs do not respond to the presence of oxygen as shown in Figure S5 of the supporting information. Many of these experiments were repeated and all materials were prepared multiple times, and in every instance, we find that these nominally O_2 sensitive dyes do not respond to oxygen when conjugated to magnetic nanomaterials.

We next sought to determine a physical reason for this phenomenon. Motivated by the well-known undergraduate demo of the capture of liquid O_2 by a magnet, the possibility of physical sequestration of oxygen by magnetic forces was studied by molecular dynamics simulation. A simplistic model was used, where a ZnS cluster with no ligands was equilibrated with a single O_2

and 2000 SPC/E water molecules under periodic boundary conditions. An equilibrated trajectory was initiated with and without the addition of a $\mu \cdot (m_{O2} \cdot m_{Mn})/r^4$ magnetic force between O_2 and a surface Zn atom site chosen to represent Mn^{2+}. Although the magnetic dipoles were modeled as perfectly aligned to provide the strongest attractive interaction, it was found that the O_2 molecule was not perturbed by a magnetic force. This is sensible as the average rms force on O_2 was found to be ~120 kJ/mol/nm as shown in Figure S6, which is overwhelmingly strong compared to a 2.6×10^{-4} kJ/mol/nm force imparted by one Mn^{2+} at a ~1 nm distance. Overall, the lack of oxygen sensitivity is unlikely due to perturbation of O_2 diffusion due to magnetic interactions.

Next, pyrene's photophysical properties were examined. First, we verified that the chemical derivatization of pyrene didn't alter the excited singlet and triplet energy splitting. Phosphoresce emission of the aminoPEG pyrene was observed at ~600 nm in water, the same as reported for neat pyrene in an aqueous micelle.[32] Regardless, this is somewhat of a non-issue as it has already been established that the singlet-triplet excited state energy splitting does not affect the ability of oxygen to quench the fluorescence of a PAH.[33] Next, the quantum yield of the dye was measured to determine whether conjugation to a magnetic QD had an effect, one that overwhelms the quenching of oxygen that might explain the lack of O_2 sensitivity. However, as shown in Table S2, there is essentially no difference in the dye's brightness due to conjugation to the magnetic quantum dot. Perturbation of the excited state dynamics of the dye was also studied. In this regard, the time-resolved emission spectra of the pyrene-QD in both magnetic and non-magnetic systems were measured in the excimer region as shown in Figure 5. In both cases nearly identical $\sim 10^{-9}$ s and $\sim 10^{-7}$ s bi-exponential decay patterns are observed, which clearly corresponds to "prompt" and delayed florescence, respectively. However, the branching ratios diverge, whereas the magnetic system has a greater delayed fluorescence dynamical component. This indicates that more pyrene

molecules in the singlet state become triplet when conjugated to Mn^{2+} doped QDs, likely due to the mixing of singlet-triplet states in the presence of a magnetic field.[34] This is possible because the excited singlet and triplet states have the proper symmetry to interact via a magnetic perturbation given the D_2h point group of the molecule, see the analysis in the SI. The question arises as to whether these differences would account for the observed lack of O_2 sensitivity. This is unlikely as increasing the singlet-triplet splitting would enhance the oxygen sensitivity rather than completely suppress it.[33] To summarize, the time resolved data demonstrate interesting differences in the dye dynamics, and the results are sensible and expected. The lack of O_2 sensitivity is not.

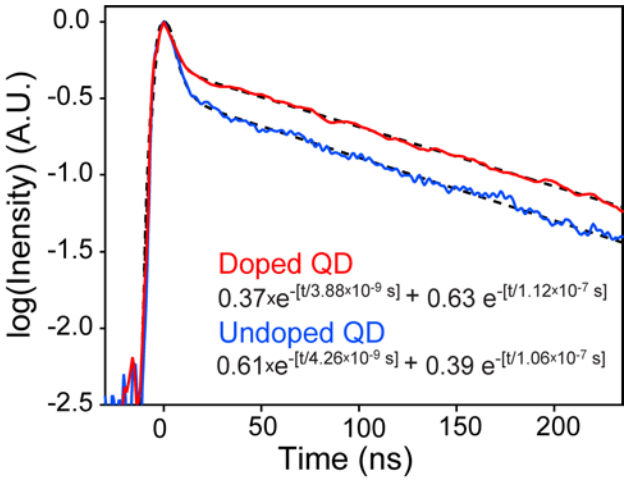

Figure 5: Time-resolved emission dynamics of pyrene in the excimer region (490 nm) conjugated to CdSe/CdZnS and CdSe/CdMnZnS QDs reveals a higher branching ratio into the delayed fluorescence channel when the dye is attached to magnetic nanomaterials. Dashed lines are fits to the data; errors are on the order of 1%.

All attempts to derive a physical basis of this phenomenon has not yielded an acceptable explanation. Furthermore, a review of the literature does not help. For example, Tachikawa and Bard reported some suppression of oxygen sensitivity of pyrene in the presence of a magnetic

field,[35] although the effect was on the order of a few percent even at very high field strengths. Several other studies have been performed on the magnetic field dependence of the triplet-triplet annihilation process that yields delayed fluorescence;[36,37] however, there is no mention of oxygen-nonsensitivity in these reports.[34] As such, there must be a disruption of the quenching process that results from both the microenvironment of the QD and a magnetic field component. Specifically, the process of O_2-induced excited state dye quenching is due to an exchange interaction[38] which is highly distance and orientation dependent.[39] This leads us to propose that the microenvironment of the QD restricts the interaction of the dye and oxygen molecule into orientations that are maximally perturbed by the magnetic field. The inhomogeneity of the magnetic field may also play a role.[40] Unfortunately, we are not aware of an experimental or theoretical method to interrogate such an interaction in a transient species.

4. CONCLUSIONS

Demonstrated here is a newly-discovered phenomenon that offers the ability to modulate the optical properties of organic chromophores using magnetic nanomaterials. Despite the mystery that envelops these observations, the effect of magnetic nanomaterial-induced loss of oxygen sensitivity has potential utility. For example, pyrene is a well-known environmentally-sensitive dye, and its use in a dye-QD platform may offer analytical development opportunities. In this regard, we have generated preliminary data that suggest pyrene-QD conjugates may be employed as ratiometric sensors for proteins, see the supporting information. Analyte selectivity for a protein such as COX-2, which is upregulated in cancer, could be created by synthesizing a three-spoke wheel motif where pyrene, a COX-2 antigen such as indocin,[41] and a QD are all conjugated together.[42] Thus, it would be advantageous to eliminate the oxygen cross-sensitivity of the dye component as shown here, especially as O_2 levels are abnormal in a cancer microenvironment.

ASSOCIATED CONTENT

Supporting Information. Additional characterization data.

AUTHOR INFORMATION

Corresponding Author

*sneep@uic.edu

Author Contributions

The manuscript was written through contributions of all authors. All authors have given approval to the final version of the manuscript.

Funding Sources

The University of Illinois at Chicago.

ACKNOWLEDGMENT

Funding from the University of Illinois at Chicago supported this work. We would like to thank L. Fung of UIC for EPR measurements.

ABBREVIATIONS

DMF, N,N-dimethylformamide; PAH, poly(aromatic) hydrocarbon; PEG, poly(ethylene glycol).

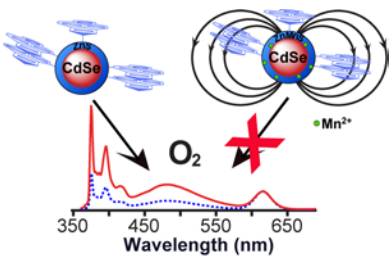

REFERENCES

1. Lane, N. *Oxygen: the molecule that made the world*; Oxford University Press: Oxford, 2003.
2. Amao, Y. Probes and Polymers for Optical Sensing of Oxygen. *Microchim. Acta* **2003,** *143*, 1-12.
3. Somers, R. C.; Bawendi, M. G.; Nocera, D. G. CdSe Nanocrystal Based Chem-/Bio- Sensors. *Chem. Soc. Rev.* **2007,** *36*, 579-591.
4. Jin, T.; Sasaki, A.; Kinjo, M.; Miyazaki, J. A Quantum Dot-Based Ratiometric pH Sensor. *Chem. Commun.* **2010,** *46*, 2408-2410.
5. Zhan, N.; Palui, G.; Mattoussi, H. Preparation of Compact Biocompatible Quantum Dots Using Multicoordinating Molecular-Scale Ligands Based on a Zwitterionic Hydrophilic Motif and Lipoic Acid Anchors. *Nat. Protocols* **2015,** *10*, 859-874.
6. Liu, L.; Hu, R.; Roy, I.; Lin, G.; Ye, L.; Reynolds, J. L.; Liu, J.; Liu, J.; Schwartz, S. A.; Zhang, X.; Yong, K.-T. Synthesis of Luminescent near-Infrared $AgInS_2$ Nanocrystals as Optical Probes for *in Vivo* Applications. *Theranostics* **2013,** *3*, 109-115.
7. McLaurin, E. J.; Greytak, A. B.; Bawendi, M. G.; Nocera, D. G. Two-Photon Absorbing Nanocrystal Sensors for Ratiometric Detection of Oxygen. *J. Am. Chem. Soc.* **2009,** *131*, 12994-13001.
8. Amelia, M.; Lavie-Cambot, A.; McClenaghan, N. D.; Credi, A. A Ratiometric Luminescent Oxygen Sensor Based on a Chemically Functionalized Quantum Dot. *Chem. Commun.* **2011,** *47*, 325-327.
9. Shamirian, A.; Samareh Afsari, H.; Hassan, A.; Miller, L. W.; Snee, P. T. *In Vitro* Detection of Hypoxia Using a Ratiometric Quantum Dot-Based Oxygen Sensor. *ACS Sensors* **2016,** *1*, 1244-1250.
10. Lemon, C. M.; Karnas, E.; Bawendi, M. G.; Nocera, D. G. Two-Photon Oxygen Sensing with Quantum Dot-Porphyrin Conjugates. *Inorg. Chem.* **2013,** *52*, 10394-10406.
11. Lemon, C. M.; Curtin, P. N.; Somers, R. C.; Greytak, A. B.; Lanning, R. M.; Jain, R. K.; Bawendi, M. G.; Nocera, D. G. Metabolic Tumor Profiling with pH, Oxygen, and Glucose Chemosensors on a Quantum Dot Scaffold. *Inorg. Chem.* **2014,** *53*, 1900-1915.
12. Lemon, C. M.; Karnas, E.; Han, X. X.; Bruns, O. T.; Kempa, T. J.; Fukumura, D.; Bawendi, M. G.; Jain, R. K.; Duda, D. G.; Nocera, D. G. Micelle-Encapsulated Quantum Dot-Porphyrin Assemblies as *in Vivo* Two-Photon Oxygen Sensors. *J. Am. Chem. Soc.* **2015,** *137*, 9832-9842.
13. Schwabacher, A. W.; Lane, J. W.; Schiesher, M. W.; Leigh, K. M.; Johnson, C. W. Desymmetrization Reactions: Efficient Preparation of Unsymmetrically Substituted Linker Molecules. *J. Org. Chem.* **1998,** *63*, 1727-1729.
14. Shen, H.; Jawaid, A. M.; Snee, P. T. Poly(Ethylene Glycol) Carbodiimide Coupling Reagents for the Biological and Chemical Functionalization of Water-Soluble Nanoparticles. *ACS Nano* **2009,** *3*, 915-923.
15. Pradhan, N.; Peng, X. Efficient and Color-Tunable Mn-Doped ZnSe Nanocrystal Emitters: Control of Optical Performance Via Greener Synthetic Chemistry. *J. Am. Chem. Soc.* **2007,** *129*, 3339-3347.
16. Snee, P. T.; Tyrakowski, C. M.; Page, L. E.; Isovic, A.; Jawaid, A. M. Quantifying Quantum Dots through Förster Resonant Energy Transfer. *J. Phys. Chem. C* **2011,** *115*, 19578-19582.
17. Thakar, R.; Chen, Y.; Snee, P. T. Efficient Emission from Core/(Doped) Shell Nanoparticles: Applications for Chemical Sensing. *Nano Lett.* **2007,** *7*, 3429-3432.

18. Berendsen, H. J. C.; Grigera, J. R.; Straatsma, T. P. The Missing Term in Effective Pair Potentials. *J. Phys. Chem.* **1987,** *91*, 6269-6271.
19. Perdew, J. P.; Burke, K.; Ernzerhof, M. Generalized Gradient Approximation Made Simple. *Phys. Rev. Lett.* **1996,** *77*, 3865-3868.
20. Adamo, C.; Barone, V. Toward Reliable Density Functional Methods without Adjustable Parameters: The PBE0 Model. *J. Chem. Phys.* **1999,** *110*, 6158-6170.
21. Stevens, W. J.; Krauss, M.; Basch, H.; Jasien, P. G. Relativistic Compact Effective Potentials and Efficient, Shared-Exponent Basis-Sets for the 3rd-Row, 4th-Row, and 5th-Row Atoms. *Can. J. Chem.* **1992,** *70*, 612-630.
22. McBride, J.; Treadway, J.; Feldman, L. C.; Pennycook, S. J.; Rosenthal, S. J. Structural Basis for near Unity Quantum Yield Core/Shell Nanostructures. *Nano Lett.* **2006,** *6*, 1496-1501.
23. Namsani, S.; Nair, N. N.; Singh, J. K. Interaction Potential Models for Bulk ZnS, ZnS Nanoparticle, and ZnS Nanoparticle-PMMA from First-Principles. *J. Comput. Chem.* **2015,** *36*, 1176-1186.
24. Grunwald, M.; Zayak, A.; Neaton, J. B.; Geissler, P. L.; Rabani, E. Transferable Pair Potentials for CdS and ZnS Crystals. *J. Chem. Phys.* **2012,** *136*.
25. Bouanich, J. P. Site Site Lennard-Jones Potential Parameters for N_2, O_2, H_2, CO and CO_2. *J. Quant. Spectrosc. Radiat. Transfer* **1992,** *47*, 243-250.
26. Parker, C. A.; Hatchard, C. G. Delayed Fluorescence of Pyrene in Ethanol. *Trans. Faraday Soc.* **1963,** *59*, 284-295.
27. Zhang, X.; Mohandessi, S.; Miller, L. W.; Snee, P. T. Efficient Functionalization of Aqueous CdSe/ZnS Nanocrystals Using Small-Molecule Chemical Activators. *Chem. Commun.* **2011,** *47*, 3532-3534.
28. Birks, J. B., *Photophysics of Aromatic Molecules*. John Wiley & Sons Ltd: New York, 1970.
29. Pradhan, N.; Goorskey, D.; Thessing, J.; Peng, X. An Alternative of CdSe Nanocrystal Emitters: Pure and Tunable Impurity Emissions in ZnSe Nanocrystals. *J. Am. Chem. Soc.* **2005,** *127*, 17586-17587.
30. Beaulac, R.; Schneider, L.; Archer, P. I.; Bacher, G.; Gamelin, D. R. Light-Induced Spontaneous Magnetization in Doped Colloidal Quantum Dots. *Science* **2009,** *325*, 973-976.
31. Chen, O.; Zhao, J.; Chauhan, V. P.; Cui, J.; Wong, C.; Harris, D. K.; Wei, H.; Han, H.-S.; Fukumura, D.; Jain, R. K.; Bawendi, M. G. Compact High-Quality CdSe-CdS Core-Shell Nanocrystals with Narrow Emission Linewidths and Suppressed Blinking. *Nat. Mater.* **2013,** *12*, 445-451.
32. Humphry-Baker, R.; Moroi, Y.; Gratzel, M. Perturbation Studies of the Photophysics of Arenes in Functionalized Micellar Assemblies. Drastic Phosphorescence Enhancements. *Chem. Phys. Lett.* **1978,** *58*, 207-210.
33. Parmenter, C. S.; Rau, J. D. Fluorescence Quenching in Aromatic Hydrocarbons by Oxygen. *J. Chem. Phys.* **1969,** *51*, 2242-2246.
34. Faulkner, L. R.; Bard, A. J. Magnetic Field Effects on Anthracene Triplet-Triplet Annihilation in Fluid Solutions. *J. Am. Chem. Soc.* **1969,** *91*, 6495-6497.
35. Tachikawa, H.; Bard, A. J. Magnetic-Field Effects on Oxygen Quenching of Delayed Fluorescence of Anthracene and Pyrene in Fluid Solution. *J. Am. Chem. Soc.* **1973,** *95*, 1672-1673.
36. Johnson, R. C.; Merrifield, R. E. Effects of Magnetic Fields on Mutual Annihilation of Triplet Excitons in Anthracene Crystals. *Phys. Rev. B* **1970,** *1*, 896-902.

37. Koehler, A.; Baessler, H. Triplet States in Organic Semiconductors. *Mat. Sci. Eng. R* **2009,** *66*, 71-109.
38. Watkins, A. R. Oxygen Quenching of the Fluorescence of Aromatic Hydrocarbons in a Polar Solvent. *Chem. Phys. Lett.* **1979,** *65*, 380-384.
39. Geacintov, N. E.; Swenberg, C. E. Possible Effects of Magnetic Fields on the Quenching of Triplet Excited States of Polynuclear Hydrocarbons by Oxygen. *J. Chem. Phys.* **1972,** *57*, 378-389.
40. Tsubomura, H.; Mulliken, R. S. Molecular Complexes and Their Spectra. XII. Ultraviolet Absorption Spectra Caused by the Interaction of Oxygen with Organic Molecules. *J. Am. Chem. Soc.* **1960,** *82*, 5966-5974.
41. Uddin, M. J.; Crews, B. C.; Ghebreselasie, K.; Marnett, L. J. Design, Synthesis, and Structure-Activity Relationship Studies of Fluorescent Inhibitors of Cycloxygenase-2 as Targeted Optical Imaging Agents. *Bioconjugate Chem.* **2013,** *24*, 712-723.
42. Tyrakowski, C. M.; Snee, P. T. Ratiometric CdSe/ZnS Quantum Dot Protein Sensor. *Anal. Chem.* **2014,** *86*, 2380-2386.